ARTICLES

An eigenfunction approach to large scale transitional structures in jet flow

L. Sirovich and M. Kirby

Center for Fluid Mechanics and Division of Applied Mathematics, Brown University, Providence, Rhode Island 02912

M. Winter

United Technologies Research Center, Hartford, Connecticut 06108

The Karhunen–Loève procedure is applied to the analysis of digitally imaged two-dimensional gas concentration fields obtained for a seeded axisymmetric jet. Large scale structures observed in the transitional region of a low Reynolds number jet are characterized in terms of an *optimal* basis. The essential features are captured by retaining roughly 30 parameters in the expansion. By retaining more terms smaller scales of the flow can be resolved.

I. INTRODUCTION

Coherent structures continue to play a central role in the discussion of transitional and turbulent flows. An excellent review of the field, as of 1981, was given by Cantwell.[1] For more recent accounts see the articles by Hussain[2,3] and Fiedler.[4] The idea that turbulent flows contain significant organized inner structure, which may have universal features, is of unquestioned appeal. It at once suggests the possibility of a simpler mathematical description, and the workings of some seemingly nonapparent physical mechanisms.

The statement that turbulent flows can contain organized structures is generally attributed to Townsend,[5] who pointed out that large scale motions are present in fully developed turbulence. A clear experimental picture of an organized structure is shown in the famous shadowgraph of the mixing layer by Brown and Roshko[6] (see also Kim, Kline, and Reynolds[7]). Visual criteria for identifying organized structures have been followed by more objective criteria, based mainly on conditional averaging and feature selection. The VITA technique of Blackwelder and Kaplan[8] (also Blackwelder and Haritonidis[9]) and the *Quadrant* analysis of Lu and Willmarth,[10] are perhaps the most important of these methods. More recently Hussain[3] and Hayakawa and Hussain[11] have suggested that large scale vorticity be used as the criterion for *educing* a coherent structure, since in their view this is the key element of a coherent structure.

A fundamental impediment to deliberations of this sort is the complete lack of an agreed on, and crisp definition of, a coherent structure. Even a widely accepted point of view as to the nature of an organized structure does not exist. An objective, statistically based procedure for the extraction of coherent structures is the proper orthogonal decomposition of Lumley.[12–14] This in turn is based on the method of Karhunen[15] and Loève[16] (K–L). However, in no instance has this procedure produced the type of structures that have appeared in experiment. Another statistical approach, and one which lies closer to experimental conditional averaging methods, has been introduced by Adrian.[17,18] Both of these approaches have been widely applied and the literature is too vast to review.

It is not our goal to assay, or to compare, the various methods that have been proposed for the extraction (or eduction) of coherent structures. Instead we start with the premise that a large scale, perhaps coherent, structure has been identified and proceed to analyze this proposed organized structure. It is our belief that the procedures that are presented here lead to a fuller and better understanding of such structures and in addition lead to efficient data reduction. Our approach should be regarded as an extension of that of Lumley,[12] but the point of view and techniques differ significantly.

All our deliberations are directed toward a series of experiments on a turbulent axisymmetric jet,[19] in which a sizable database was acquired. A description of this experiment is furnished in Sec. II.

Typical realizations of concentration fields for the seeded jet flow are shown in Fig. 1. The fluid is moving from left to right and the time sequence runs from top to bottom. We identify the large scale structures with the *blobs* that are discernible to the eye. Since the records refer to digital informa-
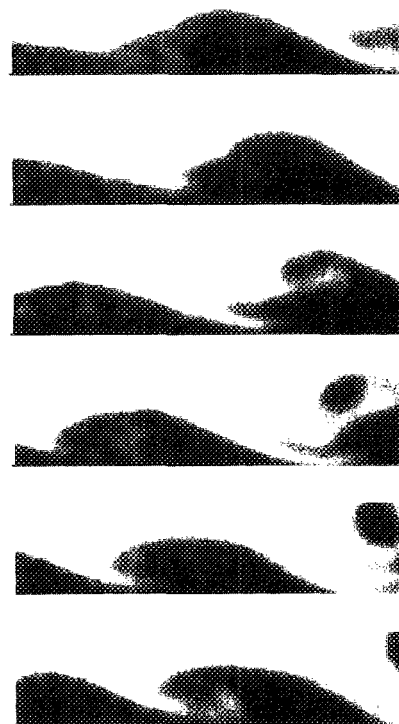

FIG. 1. Six sequential realizations taken at intervals of 0.8 msec.

tion this identification will be given an objective and precise basis. In a sense, however, we appeal to historically, the first and crudest criterion for identifying an organized structure, viz., the *eyeball norm*, but with the goal of putting this into a rational framework. An ensemble of admissible *blobs* or structures is then assembled. It is this set that is subjected to the K–L procedure and decomposed into the *eigenfunctions* of the flow. As we will show, this decomposition results in a significant data compression. A point to note is that the K–L eigenfunctions are not being represented here as the coherent structures but rather as the appropriate functions for decomposing these structures.

It is appropriate to also point out certain shortcomings and inadequacies of our results. The ensemble members, as typified by the pictures in Fig. 1, represent two-dimensional slices of the flow. As Sreenivasan[20] has shown the jet has significant azimuthal variation, and hence three-dimensional effects are being ignored. Also the ensemble members only represent concentration fields. We do not have any information on the associated mechanical motion. (Although this does not stop us from making some inferences.)

A main reason for focusing on these blemishes is so that the reader can note that the shortcomings are due to our present inability to generate more complete records. If three-dimensional full flow field records were available, the procedures that we present would be immediately applicable. This is due to our use of the *method of snapshots*,[21] which in no essential way is impeded by the potentially large records that would appear from a full three-dimensional vector resolution of a flow. Since several laboratories are now in the process of generating such complete flow records this point is of significance.

Unlike previous treatments of the K–L procedure for fluid problems, no use of homogeneous directions has been made here. Thus, we demonstrate, for the first time, the feasibility of the K–L procedure for fully three-dimensional flows. Another point to note is that the K–L procedure is being applied to a flow containing a sharp temporal frequency. It is this that leads to the conditional sampling procedure discussed in Sec. III. The recent work of Glezer *et al.*[22] also presents an extension of K–L procedure to flows lacking statistical stationarity.

II. EXPERIMENT

Recent developments in high-speed imaging techniques[19] have made it possible to follow the development of large scale structures in a turbulent jet over a wide range of Reynolds numbers. The experiment described below allows the acquisition of a large number of well-resolved flow realizations—well beyond what is practical in a comparable numerical simulation.

Instantaneous two-dimensional gas concentration fields were obtained by seeding an axisymmetric jet with submicron-sized aerosol particles and measuring the amount of light scattered from a thin sheet of copper vapor laser radiation, having wavelengths at 510 and 578 nm. A schematic of the apparatus used in the collection of the data is shown in Fig. 2. A high-speed camera (monolithic photodiode array-Reticon MC 9128) captured images of a 14 mm × 3.5 mm
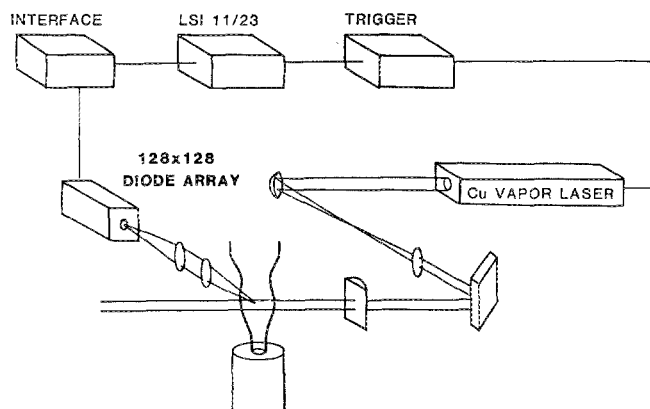

FIG. 2. Experimental apparatus for acquisition of the data.

region of the flow located at 5.25 to 8.75 nozzle diameters downstream. The camera operated at a framing rate of 1136 Hz while the laser was synchronously pulsed at 35 nsec to freeze the motion of the flow. The camera was interfaced (Microtex 7402) to a computer (LSI 11/23 with 1.25 Mbytes of high-speed memory) where images were captured in sets of 320, with pixel resolution 128 × 32 (eight bit A/D conversion at a pixel rate of 8 MHz). Figure 1 shows six measurements of gas concentration taken 0.9 msec apart. The flow is from left to right and the time sequence from top to bottom. A total of three sets of 320 images were collected for this study, all recorded at equal intervals, under the same flow conditions as described above. The raw data were corrected for background light and nonuniformities in the response of the camera and illumination sheet as detailed in Ref. 19.

Sreenivasan[20] has given an account of the characteristics of jet flow, delineating the various zones of interactions and behavior. The reader is referred to that article for details and original references. Our comments refer to the details considered here. The nozzle diameter of the jet was 4 mm, with an exit flow velocity of 4.3 m/sec, corresponding to a Reynolds number of 1150. It is known that the flow evolution is dependent on the exit conditions.[23,24] For our case the exit velocity profile was *top hat*. In earlier experiments, using the same nozzle, low turbulence levels at the nozzle were found. It was assumed that this was still the case, and no measurement of this type were made. In this same vein, since we did not record velocity fluctuations, the *potential core* was estimated from the concentration data. Using as a criterion that the rms concentration fluctuations not exceed 10% of the peak value, the tip of the potential core was found to be at roughly 7 diameters from the exit and hence in our image frame.

As has been pointed out by Hussain,[25] the jet in the image region is most susceptible to the columnar instability, which gives rise to long wavelength structures at a relatively well-defined Strouhal number. In our case the Strouhal number was 0.23 and hence about 247 structures were shed per second. At the aforementioned framing rate of 1136 Hz we see that roughly four realizations of one structure are captured in the image region.

The laser pulse duration (35 nsec) is extremely short in

comparison with the time scales just discussed, and we are well justified in regarding the realizations as instantaneous. It also follows from the above discussion that a pixel width corresponds to 10^{-4} m. A rough estimate of the Kolmogorov scale indicates that it is about a quarter of the pixel size. However, in view of the proximity of the image frame to the exit, one might expect that such small scales have not yet been established. Our later deliberations also imply this, for as we will see, modes carrying pixel-sized variations are four decades less energetic than the principal modes.

The question of particle displacement has been addressed by Long et al.[26] Using estimates given in that paper, the displacement lag of the aerosol particles is about 0.2 μm and that due to diffusion less than 0.1 μm (at 10 nozzle lengths downstream). Since the smallest scale resolved by our system is 0.1 mm, these are negligible effects. Another concern is the size distribution of seed particles, since the scattering cross section in the Lorenz–Mie domain is sensitive to particle diameter and even a small spread can produce a large change in scattered light. Our seeding density remained quite uniform as a result of our method of aerosol generation. Particles were created by atomizing a sugar–water solution. As the water evaporates, very small sugar particles are left behind. Those remaining are subjected to ionizing radiation, importing a consistent charge to prevent aggregation. Great care was also given to the density of seed particles, since high density can produce rescattered light while low density can produce a shot noise effect. Thus a delicate balance was maintained.

III. THE LARGE SCALE STRUCTURE

As mentioned in the Introduction we propose to analyze the apparent large scale structures, as depicted in Fig. 1. As a first step we develop an objective procedure for extracting these from the database acquired in the experiment. The large scale structures that appear are not fixed in space, but are convected downstream at approximately half the jet exit velocity. In addition, they appear at a roughly periodic rate given by the Strouhal number. Ideally we would like to collect ensemble members when the large scale structure is in some relatively fixed phase, perhaps at the same location in space. However, the acquisition and shedding rates are not matched, and the resulting *beat* phenomenon only seldom furnishes us with an appropriately located realization. For this reason some post-processing of the data is required.

A flow realization, giving the concentration, will be denoted by $\phi(x,y)$, or since we are dealing with discretized data,

$$\phi = \phi_{ij} = \phi(i\,\Delta x, j\,\Delta y); \quad i = 1,128; \quad j = 1,32. \quad (1)$$

A *template* is chosen from the ensemble, by taking what is considered to be a representative structure. This preselected template is shown in Fig. 3. The width of this has been *trimmed* from 128 to 70 pixels representing what we judge to be the appropriate integral scale for the structure. We denote the template by

$$f = f_{ij}; \quad i = 1,70; \quad j = 1,32. \quad (2)$$

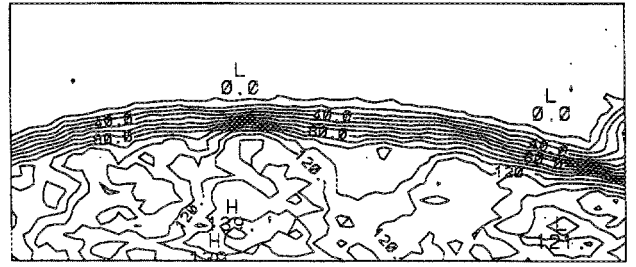For any realization, or snapshot ϕ_{ij}, there is a subportion of ϕ denoted by

FIG. 3. Template used in the conditional sampling procedure.

$$g = g_{ij}; \quad i = 1,70; \quad j = 1,32, \quad (3)$$

which is most similar to the template f, in the sense that

$$\epsilon = \int (f - g)^2 dx\,dy \quad (4)$$

is a minimum, or equivalently that the cross correlation

$$C = \int fg\,dx\,dy \quad (5)$$

is extremized. This follows procedures common to digital picture processing.[27]

For the moment it is useful to consider the full ensemble of 3 × 320 realizations as given by

$$\{\phi^m\} = \phi_{ij}(m). \quad (6)$$

The method then consists of taking for each m, the normalized cross correlation

$$B^{(k)}(m) = \frac{\Sigma_{ij} f_{ij} \phi_{i+k,j}(m)}{(\Sigma_{ij} f_{ij}^{(2)})(\Sigma_{ij} \phi_{i+k,j}^2)}, \quad (7)$$

where $i = 1,70$ and $j = 1,32$. Each realization is *slid* over the template by varying k until a maximum is obtained

$$B(m) = \max_{1 \leq k \leq 58} B^{(k)}(m). \quad (8)$$

The corresponding subportion of the realization that yields the maximum will henceforth be denoted now by $\phi_{ij}^{(m)}$.

Actually, since the framing rate of the camera was set such that a typical structure was imaged about four times, we are including snapshots of the same structure in different stages of development. We therefore choose only those that correspond to a local maximum of $B(m)$, i.e., best correlated to the template. In this way we generate an ensemble of roughly $\frac{1}{4} \times 3 \times 320$ snapshots. In what follows we regard the ensemble

$$\phi = \{\phi_{ij}^{(m)}\} \quad (9)$$

as containing $M = 210$ members. The remaining snapshots have been reserved for later comparison purposes. Thus the ensemble members (9) correspond to the local maxima of (8) and further are *cropped* to 70 × 32 pixels reflecting the integral scale of the structure.

With the ensemble (9) thus constructed, we can compute the ensemble average,

$$\bar{\phi}_{ij} = \langle \phi_{ij} \rangle = \sum_{m=1}^{M} \phi_{ij}^{(m)} \quad (10)$$

($M = 210$), which is depicted in Fig. 4. This in turn can be used as a *better* template and the process repeated. This re-
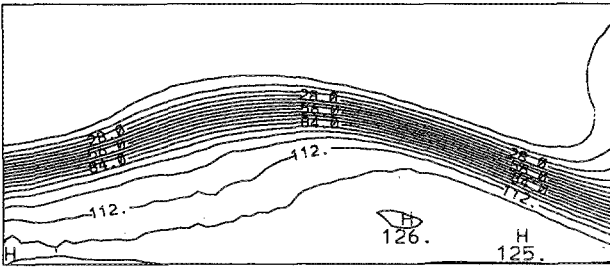
FIG. 4. Ensemble average taken over 210 concentration fields.

sults in only minor changes in the decomposition that is presented next.

The procedure just described for identifying a large scale structure makes use of a conditional sampling criterion. Namely, that out of the roughly four snapshots in a sequence, we choose the snapshot that is closest to some preselected *phase* of the structure. This approach was adopted because the jet phenomenon is statistically unsteady. As a result of the Strouhal frequency the power spectrum has a sharp peak. If many snapshots were available for each period, instead of just four, we could generate an ensemble for each of a number of selected phases in a period. We return to this point again in the next section.

IV. KARHUNEN–LOÈVE PROCEDURE

The details of the Karhunen–Loève (K–L) procedure can be found in textbooks.[14,28] The brief outline given here follows that given in Ref. 21, in which the *snapshot method* is presented. For purposes of exposition, it is useful to regard the ensemble members as defined over continuous variables

$$\phi^{(m)} = \phi^{(m)}(x,y). \tag{11}$$

As is customary, it proves efficient to remove mean quantities. Thus, instead of (11) we consider

$$\varphi^{(m)} = \phi^{(m)} - \bar{\phi}, \tag{12}$$

where $\bar{\phi}$ is defined by (9).

The covariance is defined by

$$C(x,y;x',y') = \langle \varphi(x,y)\varphi(x',y') \rangle$$
$$= \frac{1}{M}\sum^{M} \varphi^{(m)}(x,y)\varphi^{(m)}(x',y'), \tag{13}$$

where M is the number of ensemble members ($M = 210$).

The K–L basis is obtained by solving for the eigenfunctions u in

$$\int C(x,y;x',y')u(x',y')dx'dy' = \lambda u(x,y), \tag{14}$$

where the integration is over the domain of interest. It may be shown that (14) generates a complete set of eigenfunctions. In view of the possible size of the database, it might be supposed that solution of (14) would be out of reach of presently available computers. However, (13) implies that C is a degenerate kernel, and as a result we can express the eigenfunctions as an admixture of the *snapshots*,

$$u(x,y) = \sum_{n=1}^{M} a_n \varphi^{(n)}(x,y). \tag{15}$$

When this is inserted into (14) this leads to an ($M \times M$) matrix eigenvector problem, which in the present instance is relatively simple computational to solve. [This generates all eigenfunctions of (14) with possible nonzero eigenvalues.] For a related application in pattern recognition see Refs. 29 and 30.

The K–L basis of orthonormal eigenfunctions will be denoted by $\{u^{(k)}(x,y)\}$ and the corresponding eigenvalues by $\{\lambda_k\}$. It may be shown that the K–L basis is optimal in the sense that of all orthonormal bases, the K–L basis gives, on average, the best approximation to the snapshots $\{\varphi^{(m)}\}$ for any specified number of terms. Specifically for any N, and

$$\varphi_N = \sum_{n=1}^{N} a_n u^{(n)} \tag{16}$$

with

$$a_n = (u^{(n)},\varphi) = \int u^{(n)}\varphi, \tag{17}$$

the error

$$e_N = \langle \|\varphi - \varphi_N\|^2 \rangle$$

is minimal, if the $\{u^{(k)}\}$ in (16) are the K–L eigenfunctions. [The norm $\| \ \|$ is defined by the inner product (17).]

Any snapshot (9) may now be represented in terms of the K–L basis. We term a *reconstruction* as the fitting of a member of the ensemble to the basis set, and an *approximation* as the projection of a flow realization onto the basis, with the understanding that it was not used in computing the covariance matrix (it being one of the snapshots that were reserved for this purpose). This distinction will be useful in assessing the success of the method and actually will provide both an upper and lower bound on the actual mean-square error.

A full reconstruction is exact since in this case the method just corresponds to a linear change of basis and the eigenfunctions of the form (15) are complete for the ensemble used to construct C. Hence, capturing the features of an ensemble member is guaranteed, and only the rate of convergence is an issue. However, if we consider an arbitrary flow, the basis furnished by (15) is not complete. Thus an approximation gives valuable information regarding the extent to which we have spanned the space of admissible solutions by our basis. The mean-square error for the approximations should be considered an upper bound on the error, which decreases in general as the size of the ensemble increases.[30] We expect the distinction between a reconstruction and approximation to diminish as the ensemble size increases. The true mean-square error for the reconstructions (or approximations) will be achieved when the ensemble size is large enough, i.e., when it spans the entire set of admissible snapshots.

For any snapshot, ϕ, in or out of the ensemble, we write,

$$\phi_N = \bar{\phi} + \varphi_N, \tag{18}$$

where φ_N is defined by (16). The mean-square error is then given by

$$\epsilon_N = \|\phi - \phi_N\|^2 / \|\phi\|^2. \tag{19}$$

The K–L procedure is now applied to the ensemble of snapshots that was generated by the selection procedure discussed in Sec. III. Since the ensemble members were conditionally sampled the method that we are describing departs somewhat from the standard K–L procedure. We are actually determining the eigenfunctions for a particular *phase* of the large scale structure. If, as pointed out in the previous section, we had ensembles for each of a number of the phases in a typical period, then eigenfunctions at each phase could be determined. In this way a set of time dependent K–L *eigenfunctions* could be determined.[31]

V. RESULTS

The result of computing the ensemble average, (10), with $M = 210$ members, is shown in Fig. 4. We see that the internal features are smoothed and that the averaged structure appears to have a *roll* feature on the downstream side of the frame. In Fig. 5 we show two typical snapshots chosen at random, paired with their mean subtracted realizations. The first pair, 5(a) and 5(b), is used in computing the eigenfunctions; the second, 5(c) and 5(d), is one of the reserved set not belonging to the ensemble. We will use these to evaluate the ability of the method to reconstruct and approximate arbitrary flows.

A. Eigenvalues

The result of determining the eigenvalues, λ_k, (14), normalized by the total *energy* or variance,

$$E = \langle (\varphi, \varphi) \rangle = \sum_k^M \lambda_k, \qquad (20)$$

is plotted in Fig. 6(a). Since λ_k / E is being plotted the area under the curve is unity, i.e., λ_k / E gives the probability that the large scale structure fall in the direction of the eigenfunction u_k. The *integral* of the curve in 6(a),

$$E_N = \sum_{k=1}^N \frac{\lambda_k}{E} \qquad (21)$$

is shown in Fig. 6(b), and measures the average amount of *energy* or variance that is captured as a function of the number of modes. A useful concept is that of intrinsic dimension, viz., the number of modes on average needed to satisfy some criterion level of approximation. In the context of fluid problems, it has been suggested that this be determined by the requirement that 90% of the variance be captured and that $\lambda_k / \lambda_{\max} < 0.01$, for $k > N$.[32] This K–L dimension in the present instance is about 40, part of which can be seen from Fig. 6(b).

Both curves in Fig. 6 show a *break* in slope at about an eigenvalue index of 30. The same sort of behavior will be shown later when we approximate realizations from outside of the ensemble. We might conclude from this that there are two rates of convergence, each corresponding to a different leg of the curve. Clearly we capture information, on average, most rapidly until about 30 terms; after this the rate of convergence for both the reconstruction and approximation falls off. As we will see the second leg corresponds to the less resolved or *noisy* eigenvalues. This suggests that roughly the
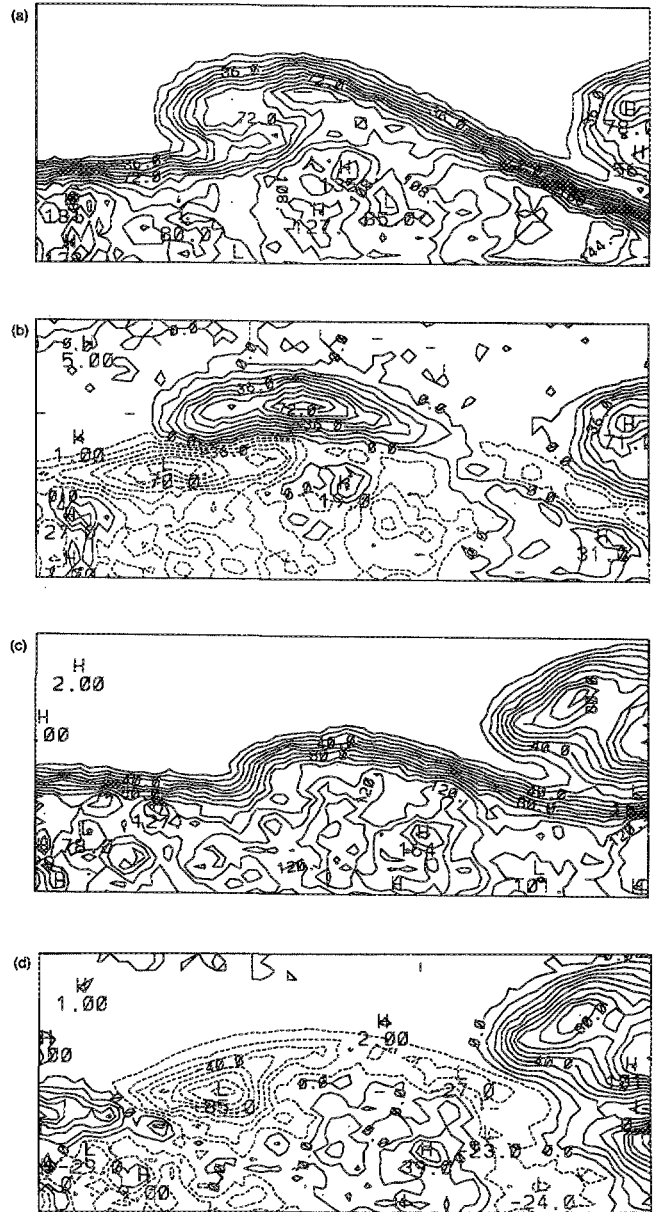

FIG. 5. (a) Typical coherent structure resulting from the sampling procedure. (b) Fluctuating concentration field for realization (a). (c) Another typical realization resulting from the sampling procedure. This snapshot is not used in computing the eigenfunctions. (d) Fluctuating concentration field for realization (c).

first 30 eigenfunctions are well resolved by our database while the remaining are not yet fully resolved.

B. Eigenfunctions

The first five eigenfunctions resulting from the solution of (14) are shown in Fig. 7 and in false color in Fig. 8. Taken together these five represent 54% of the variance of the ensemble. The form and structure of these eigenpictures remained essentially unchanged as the ensemble size was varied over 70, 150, and 210 members. This is in keeping with the observation, in the previous paragraph, that the principal eigenfunctions are well determined by relatively small populations. It also infers that the template matching and
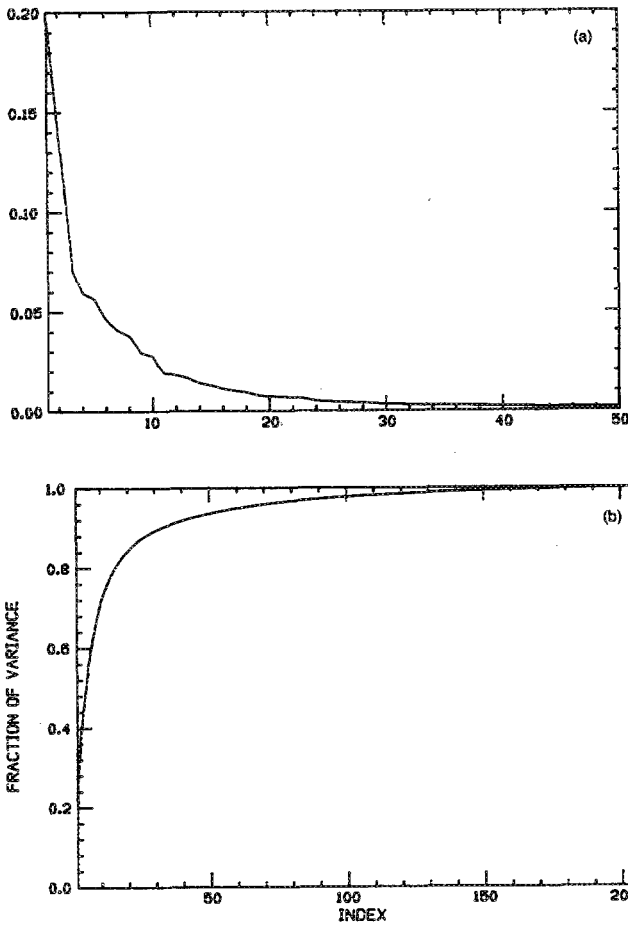
FIG. 6. (a) Normalized eigenvalues $\lambda_k/\Sigma\lambda_k$ vs k. (b) Fraction of total variance E_N vs N.

FIG. 7. Eigenfunctions corresponding to the five largest eigenvalues. Taken together they account for 54% of the total variance.

conditional sampling procedures lead to a well-defined space of principal eigenfunctions. In viewing Fig. 7, no significance should be attached to the relative magnitude of the features of the eigenfunction since multiplication by a constant does not alter the eigenfunction property.

The first eigenfunction, representing 20% of the variance, has three identifiable large scale features. A negative extremum in the center, flanked by a maximum on either side, at roughly 75% and 50% the amplitude of the minimum. Clearly they play a role in the description of the structure of the material interface, i.e., its location, and the nature of the *roll* feature. The next eigenfunction, representing 14% of the variance, has more internal structure but the most significant feature is the narrow band of large amplitude that outlines the boundary of the structure. There are two identifiable extrema on the interface, roughly on opposite sides of the flow frame. We note that, in contrast with the first eigenfunction, the extrema are of the same sign. Note also that there is a roll structure in the upper right corner of the frame with about 25% the magnitude of the largest extremum. The first eigenfunction to have significant internal structure is number three. The number of extrema is up to five by the fourth eigenfunction and we see that the important features are both internal and relevant to the boundary. The fifth is
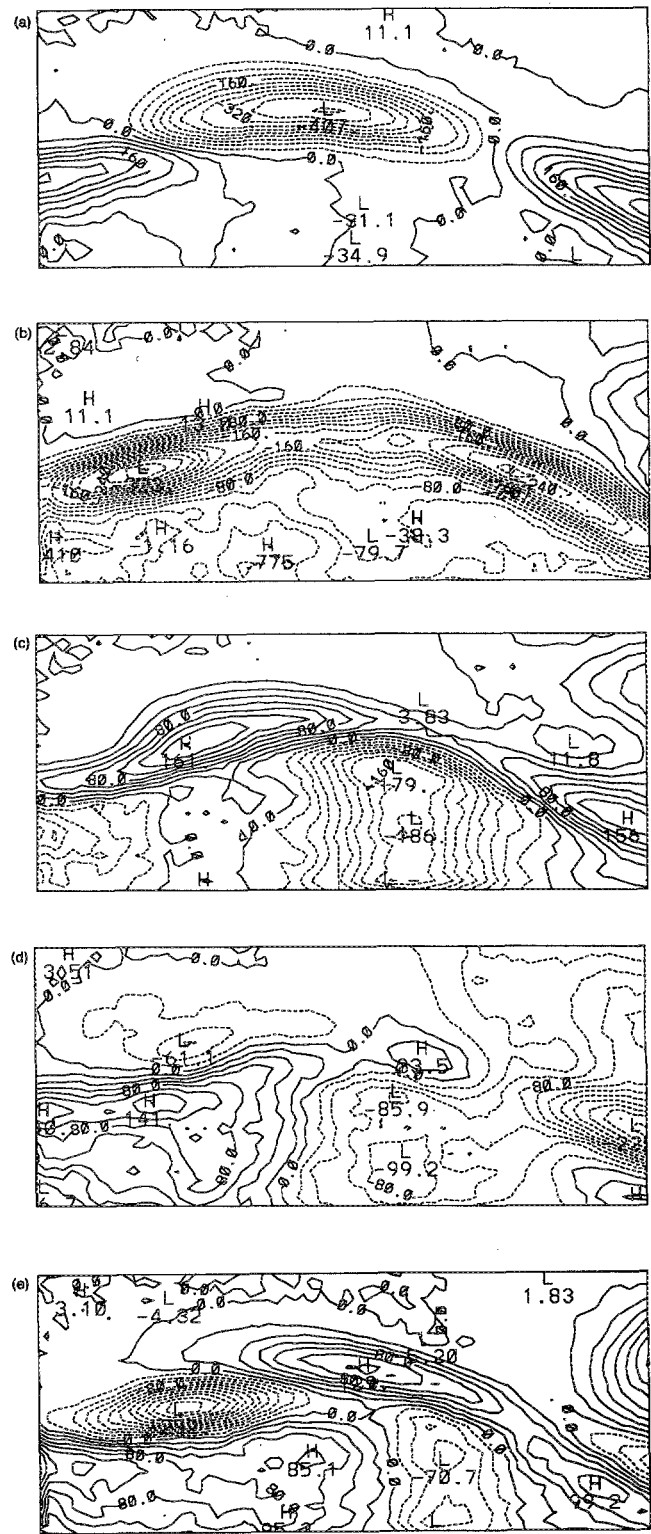
clearly important for representing the roll-up type structure that is observed in the ensemble average.

As the index increases so does the fine structure of the corresponding eigenfunction. This is illustrated by the sixth panel of Fig. 8, which displays the 200th eigenfunction. As can be seen from this illustration the scale is beginning to
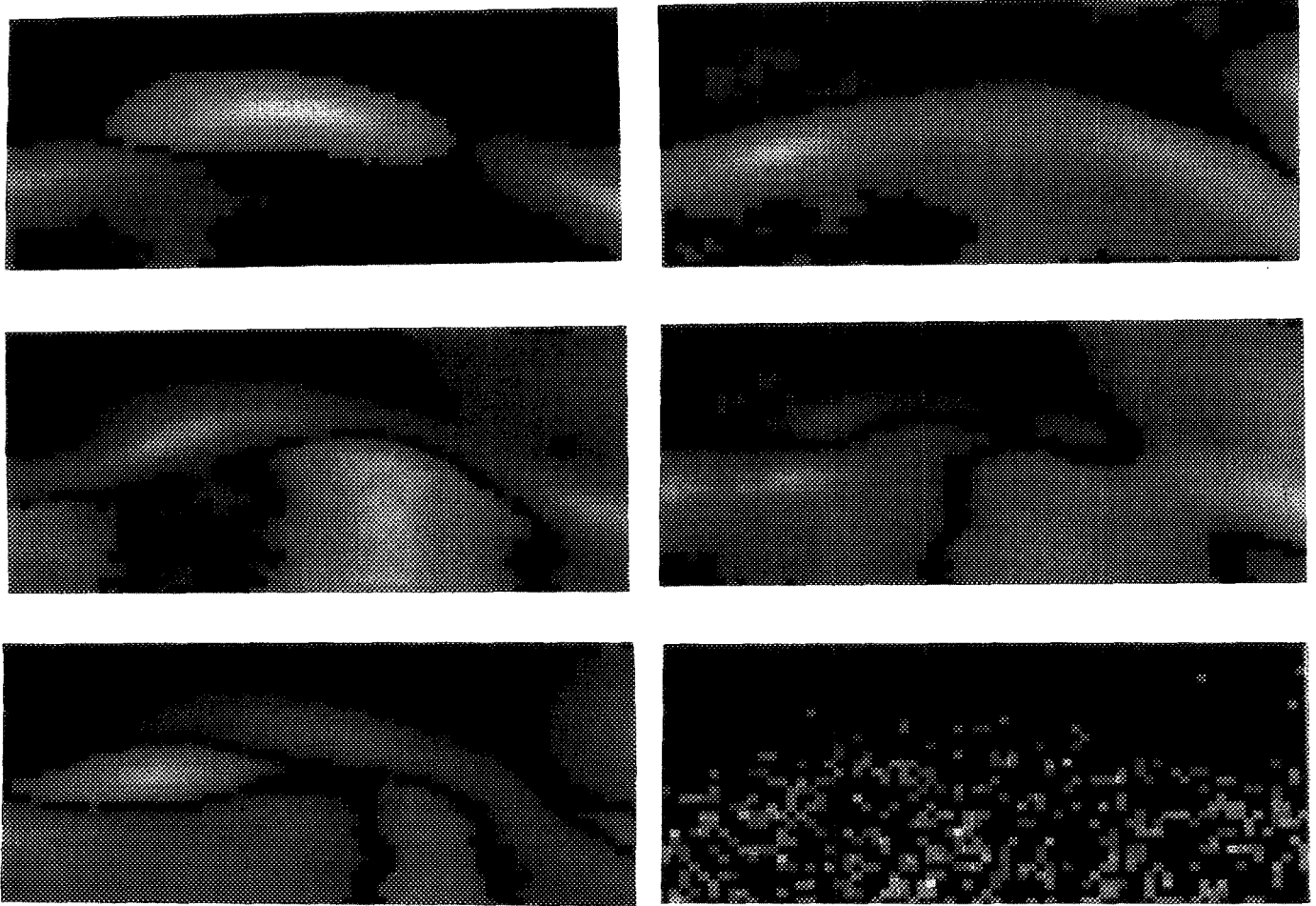
FIG. 8. Eigenfunctions corresponding to the first five largest eigenvalues, in order from left to right and top to bottom. *Noisy* eigenfunction in bottom right corner corresponds to 200th largest eigenvalue.
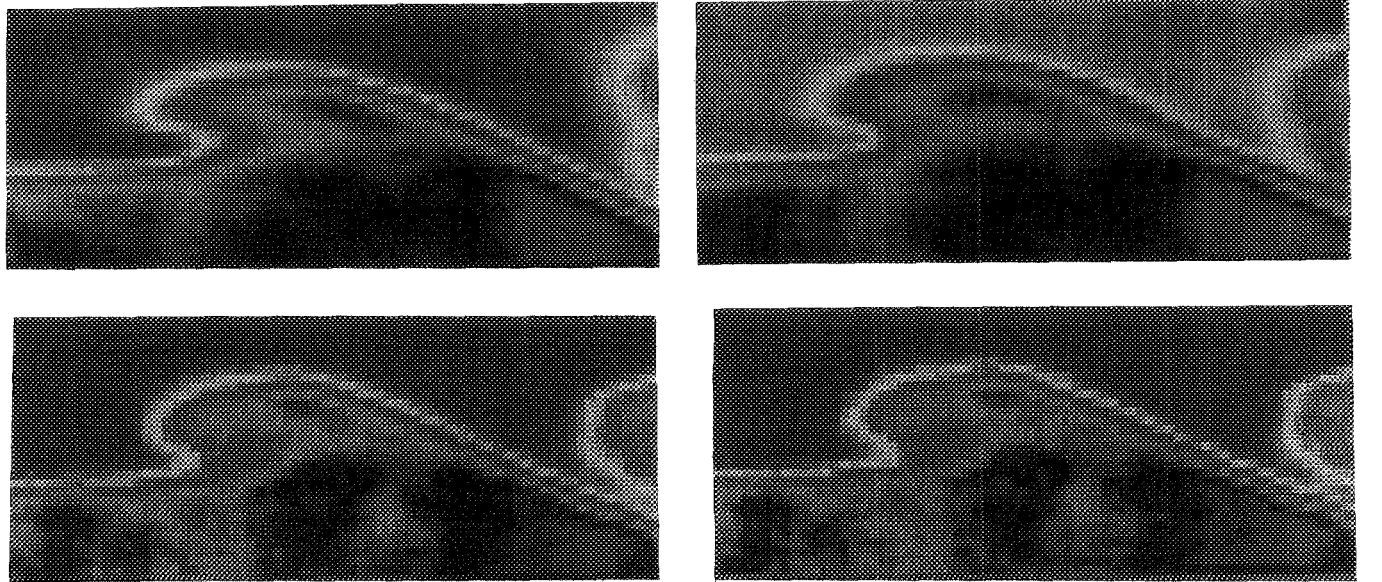

FIG. 9. Reconstruction of snapshot shown in Fig. 5(a) for 10 (upper left corner), 20 (upper right), and 100 (lower left) terms. The flow begin reconstructed is in the bottom right corner.

pick up individual pixels. As Fig. 6 illustrates, the corresponding energy at this index is insignificant, and in fact is less than 0.01%. This also addresses the question posed earlier as to whether the resolution is adequate for the smallest structures. Indeed, modes carrying individual pixel variations account for negligible variations in the mean-square variation of the concentration.

C. Reconstruction and approximations

We consider two examples in the following: a typical reconstruction of a member of the ensemble, and the approximation of a typical nonensemble flow field. The former is depicted in Fig. 9. Viewing this we see that ten terms are sufficient to capture the gross structure of the flow. The error as measured by (19) is 13%. At 100 terms this is down to 3%. This accuracy is to be expected in view of the fact that the full reconstruction is *exact*. However, even at 20 terms detailed structure is resolved, e.g., the *roll* in the right of the frame is recovered, and by 100 terms most of the small scales are accurately captured as can be seen in the detail given in Fig. 10. Perhaps more surprising are the results of the approximation to the nonensemble member. Although it now takes more terms to capture all the features, we see from Fig. 11 that 20 terms are sufficient to recreate the large scales, and up to 150 terms capture much of the small scale features. The corresponding errors for these figures are 17% and
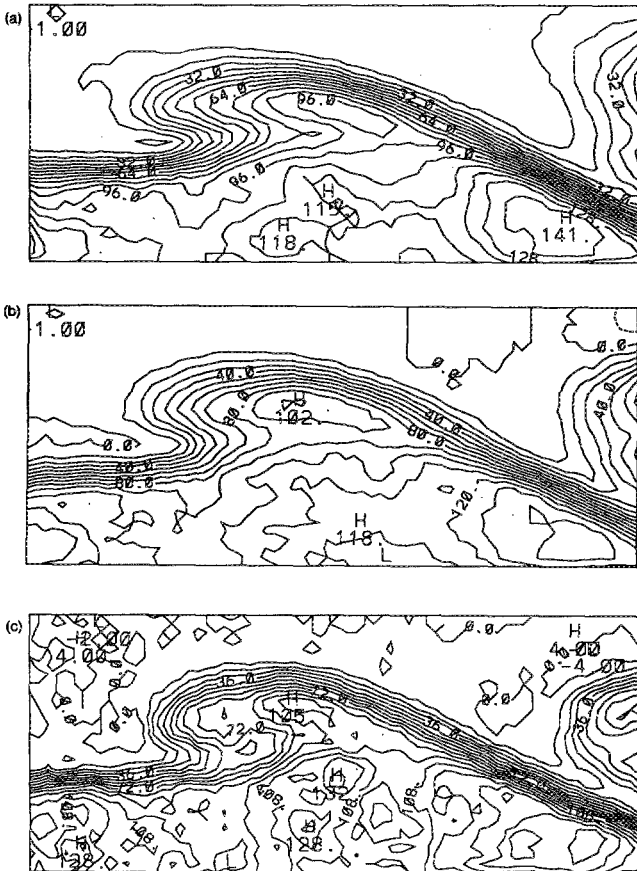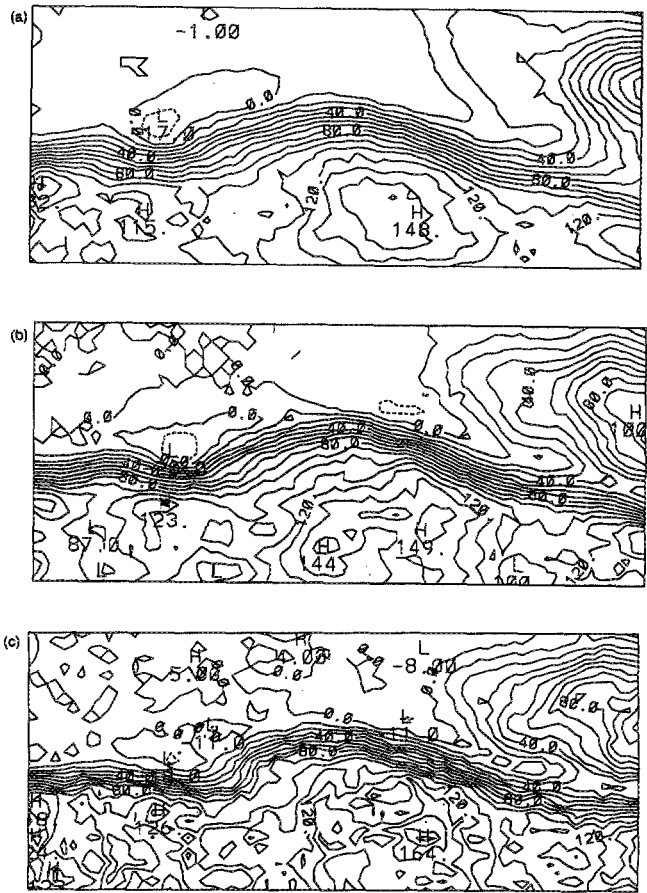

FIG. 11. Approximation of realization shown in Fig. 5(c) for (a) 20, (b) 40, (c) 150 terms.

9.9%, respectively. The approximation error ϵ_N, averaged over 11 realizations, and the convergence errors for both Figs. 10 and 11 are shown in Fig. 12. Note that the convergence errors for Fig. 11 are considerably larger than average.
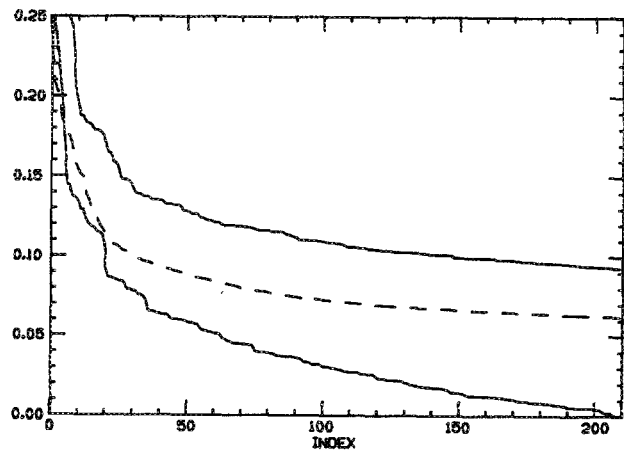

FIG. 12. Dashed curve gives approximation error ϵ_N averaged over 11 realizations selected at random. The upper solid curve gives the error ϵ_N for the flow shown in Fig. 5(c). The lower solid curve gives the reconstruction error for Fig. 5(a).

FIG. 10. Reconstruction of realization shown in Fig. 5(a) for (a) 10, (b) 20, (c) 100 terms.

134   Phys. Fluids A, Vol. 2, No. 2, February 1990

Sirovich, Kirby, and Winter   134

VI. DISCUSSION

The approach presented here, for characterizing the large scale structures, allows us to view the jet flow realizations in terms of the superposition of a number of eigenfunctions. If it is accepted that the method captures the gross features of the flow with approximately 30 terms, then this corresponds to a data compression factor of roughly 70:1. This is based on the rough estimate that 70×32 pixels depict a large scale structure. We expect that this estimate would not be altered significantly if the ensemble size increased or even became unbounded. There are two reasons for this assertion. First it should be noted that the subensembles of 70 and 150 showed no significant alteration of the principal eigenfunctions. Thus, although an increase in the ensemble size would sharpen the eigenfunctions in the *tail*, i.e., as the index is increased, little alteration of the earlier eigenfunctions should be expected. Second we observed that realizations outside the population were well fit by the first 30 to 40 eigenfunctions, i.e., the average percent error was about 10%. Moreover we expect this to show some improvement with increasing ensemble population.[30]

A related point is concerned with the 70×32 pixel resolution. Although this was deemed adequate to resolve the flow at the flow Reynolds number, one can imagine increasing the resolution (perhaps just for cosmetic purposes). The above discussion strongly implies that the number of relevant eigenfunctions will not change to any significant degree. They will only become smoother in appearance.

As we pointed out in the Introduction, a shortcoming of the current investigation is that we consider a two-dimensional slice of what is truly a three-dimensional flow. It has been observed that as we proceed along the transition region, the flow becomes increasingly three-dimensional due to instability of the vortices.[20,33] From the development presented in this paper it is clear that three-dimensional realizations can be handled without difficulty. Thus, advances in technology that are now taking place, and that lead to three-dimensional fields, can be treated virtually without change by the methodology of this paper. Another extension of the methodology would be to factor into the procedure the underlying periodic nature of the flow. This has been discussed in Secs. III and IV and further discussion is not deemed necessary.

Another shortcoming of the above treatment is our limited ability in interpreting the concentration patterns in terms of the actual motions. Since several laboratories are now engaged in developing techniques for simultaneously generating velocity and concentration data, we briefly comment on the required extension. To treat such a case it is only necessary to adapt the formalism to vector fields.[21,31,32] Thus instead of scalar snapshots, (11) or (12), we use vector snapshots composed of the velocities and concentration. Instead of a scalar covariance, (13), we now obtain a matrix covariance. The application of the snapshot method can then be applied almost without change. This approach has been taken with a numerical simulation of the allied problem of axisymmetric jet flow.[34] It was found there that concentration fields can be indeed related to the mechanical motions.

We close by summarizing the major contributions of this paper: (1) The development of a methodology for analyzing and treating large experimental and numerical databases. (2) Demonstration that the K–L procedure can be applied with present computer power, to fully inhomogeneous three-dimensional turbulence. (3) New ideas to pursue in order to gain a deeper understanding of coherent structures. In this context it is interesting to observe that Moin and Moser[35] using admixtures of K–L eigenfunctions create what they term *characteristic eddies*, which do bear a resemblance to accepted coherent structures. (4) Demonstration that tracer particles in a fluid provide much more information than just gross features such as boundaries.

[1] B. J. Cantwell, Annu. Rev. Fluid Mech. **13**, 457 (1981).
[2] A. K. M. F. Hussain, Phys. Fluids **26**, 2816 (1983).
[3] A. K. M. F. Hussain, J. Fluid Mech. **173**, 303 (1986).
[4] H. E. Fiedler, in *Proceedings Advances in Turbulence*, edited by G. Comte-Bellot and J. Mathieu (Springer, Berlin, 1987), pp. 320–336.
[5] Townsend, *The Structure of Turbulent Shear Flow* (Cambridge U.P., Cambridge, 1956).
[6] G. L. Brown and A. Roshko, J. Fluid Mech. **64**, 775 (1974).
[7] H. T. Kim, S. J. Kline, and W. C. Reynolds, J. Fluid Mech. **50**, 133 (1971).
[8] R. F. Blackwelder and R. E. Kaplan, J. Fluid Mech. **76**, 89 (1976).
[9] R. F. Blackwelder and J. H. Haritonidis, J. Fluid Mech. **132**, 87 (1983).
[10] S. S. Lu and W. W Willmarth, J. Fluid Mech. **60**, 481 (1973).
[11] M. Hayakawa and A. K. M. F. Hussain, in *Proceedings of the 5th Symposium on Turbulent Shear Flow, Cornell Univ.* (Springer, Berlin, 1985), pp. 4.33–4.37.
[12] J. L. Lumley, in *Atmospheric Turbulence and Radio Wave Propagation*, edited by A. M. Yaglom and V. I. Tatarski (Nauka, Moscow, 1967), pp. 166–178.
[13] J. L. Lumley, in *Transition and Turbulence*, edited by R. E. Meyer (Academic, New York, 1981), pp. 215–242.
[14] J. L. Lumley, *Stochastic Tools in Turbulence* (Academic, New York, 1970).
[15] K. Karhunen, Ann. Acad. Sci. Fennicae, Ser A **1**, Math. Phys. **37**, 1(1946).
[16] M. M. Loève, *Probability Theory* (Van Nostrand, Princeton, NJ, 1955).
[17] R. J. Adrian, in *Proceedings of the 4th Biennial Symposium of Turbulence in Liquids*, edited by J. L. Zakin and C. K. Patterson (Scientific, Princeton, NJ, 1977), pp. 323–332.
[18] R. J. Adrian, Phys. Fluids **22**, 2065 (1979).
[19] M. Winter, J. K. Lam, and M. B. Long, Exp. Fluids **5**, 177 (1987).
[20] K. R. Sreenivasan, Phys. Fluids **27**, 867 (1984).
[21] L. Sirovich, Q. Appl. Math. **45** (3), 561 (1987).
[22] A. Glezer, Z. Kadioglu, and A. Pearlstein, Phys. Fluids A **1**, 1363 (1989).
[23] P. Bradshaw, J. Fluid Mech. **26**, 225 (1966).
[24] A. K. M. F. Hussain and M. F. Zedan, Phys. Fluids **21**, 1475 (1978).
[25] A. K. M. F. Hussain and K. B. M. Q. Zaman, J. Fluid Mech. **110**, 39 (1981).
[26] M. B. Long, B. T. Chu, and R. K. Chang, AIAA J. **19**, 1151 (1981).

[27] A. Rosenfeld and A. C. Kac, *Digital Picture Processing* (Academic, New York, 1982).

[28] R. B. Ash and M. F. Gardner, *Topics in Stochastic Processes* (Academic, New York, 1975).

[29] L. Sirovich and M. Kirby, J. Opt. Soc. Am. A **4**, 519 (1987).

[30] J. Kirby and L. Sirovich, IEEE Trans. Pattern Anal. Machine Intell. **12**, 103 (1990).

[31] L. Sirovich, Physica D **37**, 126 (1989).

[32] L. Sirovich, *Low Dimensional Description of Complicated Phenomena*, Contemporary Mathematics, edited by B. Nicolaenko, (Am. Math. Soc., Providence, RI, 1988).

[33] A. J. Yule, J. Fluid Mech. **89** (pt. 3), 413 (1978).

[34] M. Kirby, J. Boris, and L. Sirovich, J. Comput. Phys. (in press).

[35] P. Moin and R. Moser, J. Fluid Mech. **200**, 471 (1989).